**RESEARCH PAPER**

# A study to determine the impact of IMPT optimization techniques on prostate synthetic CT image sets dose comparison against CT image sets

Gipson Joe Anto[1], Sureka Sekaran[1], Bojarajan Perumal[1], Natarajan Ramar[2], Vaitheeswaran R[1], Karthikeyan SK[1]

[1]Department of Medical Physics, Bharathiar University, Coimbatore, India
[2]Department of Physics, School of Advanced Sciences, Vellore Institute of Technology, Vellore, India

## ABSTRACT

**Background:** The objective of this study is to determine the impact of intensity modulated proton therapy (IMPT) optimization techniques on the proton dose comparison of commercially available magnetic resonance for calculating attenuation (MRCAT) images, a synthetic computed tomography CT (sCT) based on magnetic resonance imaging (MRI) scan against the CT images and find out the optimization technique which creates plans with the least dose differences against the regular CT image sets.

**Material and methods:** Regular CT data sets and sCT image sets were obtained for 10 prostate patients for the study. Six plans were created using six distinct IMPT optimization techniques including multi-field optimization (MFO), single field uniform dose (SFUD) optimization, and robust optimization (RO) in CT image sets. These plans were copied to MRCAT, sCT datasets and doses were computed. Doses from CT and MRCAT data sets were compared for each patient using 2D dose distribution display, dose volume histograms (DVH), homogeneity index (HI), conformation number (CN) and 3D gamma analysis. A two tailed t-test was conducted on HI and CN with 5% significance level with a null hypothesis for CT and sCT image sets.

**Results:** Analysis of ten CT and sCT image sets with different IMPT optimization techniques shows that a few of the techniques show significant differences between plans for a few evaluation parameters. Isodose lines, DVH, HI, CN and t-test analysis shows that robust optimizations with 2% range error incorporated results in plans, when re-computed in sCT image sets results in the least dose differences against CT plans compared to other optimization techniques. The second best optimization technique with the least dose differences was robust optimization with 5% range error.

**Conclusion:** This study affirmatively demonstrates the impact of IMPT optimization techniques on synthetic CT image sets dose comparison against CT images and determines the robust optimization with 2% range error as the optimization technique which gives the least dose difference when compared to CT plans.

**Key words:** IMPT; MRCAT; synthetic CT; SFUD; MFO; robust optimization

*Rep Pract Oncol Radiother 2022;27(1):161–169*

## Introduction

Historically, computed tomography (CT) images have been used as primary images in radiation oncology treatment planning as it provides electron density information in the form of CT numbers for dose computation. Other imaging modalities like magnetic resonance imaging (MRI), positron

emission tomography (PET), and single-photon emission computed tomography (SPECT), are used as secondary images for their resolution and functional imaging advantages. MRI scanning modality offers superior soft tissue contrast for target and organ at risk (OAR) delineation and dynamic imaging techniques for motion management, without any radiation dose [1]. However MRI doesn't have electron density information for dose computation it becomes necessary to impose two scans on patients resulting in additional burden on patients and clinical personnel. Other downsides of multiple scans are registration challenges caused by the difference in scanner hardware and patient anatomy changes between the scans and the additional radiation dose to patients due to CT scan [2]. The registration of image modalities is expected to match within error tolerances set to 2 to 3 mm target registration error (TRE) and 0.80 to 0.90 dice similarity coefficient (DSC) [1].

These challenges led to the emergence of synthetic CT (sCT); CT equivalent images derived from non-CT modalities with CT number information. MRI is a widely used imaging modality to create synthetic CT images. There are a few algorithms available to derive synthetic CT images from MRI scans, namely bulk density assignment, registration and atlas-based approach, regression, classification or direct approach and hybrid approach [3, 4]. Bulk density approach involves segregating tissue type and assigning homogeneous CT density to them [4, 5]. Registration and atlas-based approach employs rigid and deformable mapping of Hounsfield number onto an MRI scan [5]. Regression, classification, or direct approaches aim to characterize tissue properties directly from MR image intensities [6]. Hybrid approach is a combination of atlas and regression methods for CT density approximation for MR images with higher prospects [7, 8]. Magnetic resonance for calculating attenuation (MRCAT) [9] is a commercially available sCT algorithm for male pelvis anatomy developed by Philips medical systems, Helsinki, Finland to derive sCT from MRI scans.

The MRCAT sCT algorithm was validated for dose computation of photon beams in radiotherapy treatment planning with suitable CT to density table and recommended for clinical use [3, 10–14]. There were also studies performed on dose accuracy of proton beams on the sCT images [9, 15].

A study by Nicolas Depauw et al. on MRCAT prostate sCT algorithm encourages intensity modulated proton therapy (IMPT) treatment planning on the sCT images clinically [15].

IMPT has become an established method for treating cancer using proton pencil beams. IMPT technique optimizes the weights of each pencil of the proton beam to achieve the clinical goals. IMPT can create plans with highly conformal and homogeneous dose distribution to a geometrically complex tumor while sparing doses to adjacent organs at risk (OAR) [16]. IMPT plans have high dose gradients which are highly sensitive to setup and proton beam range errors [17, 18]. Range errors might be caused by uncertainty in CT Hounsfield units' conversion to stopping power, artifacts in the CT image, and patient anatomical changes [16]. A few optimization techniques were developed to reduce the uncertainties in the treatment delivery, namely single field uniform dose (SFUD) and robust optimization (RO) [16–19]. Conventional IMPT optimization without any above additional constraints are termed as multi field optimization (MFO) [17, 20].

SFUD optimization was designed to make the plan robust to range error and/or any setup error [8, 17, 18]. It is similar to MFO with an additional goal of delivering a uniform dose to target volume from each beam. This technique creates plans with uniform dose to target from each beam [16–18] and may result in sub-optimal organ at risk sparing, especially for OARs closer to targets [17, 18]. In RO formulation of the IMPT planning problem, geometric uncertainty is modeled as uncertainty in the dose-fluence matrix [18]. The optimizer is given additional constraints aimed to reduce the difference between the plans in the treatment planning system and the delivered plan [19]. Plan quality may be compromised relative to the MFO plans as the high dose gradients are smudged [18, 20]. Each optimization technique creates a signature pattern of dose distribution in the patient image sets [18, 20].

Main purposes of this study were to determine whether the optimization techniques of IMPT have any impact on the dosimetric comparison of MRCAT synthetic CT against regular CT images and determine the parameters or optimization constraints, which helps to reduce the dosimetric differences between them. This is a comparative study

between different optimization techniques of IMPT with little focus on absolute dosimetric accuracy of IMPT beams on MRCAT sCT image sets.

## Materials and methods

Regular planning CTs of ten prostate cancer patients in a supine position with 2 mm slice thickness and $1 \times 1$ mm$^2$ in-plane resolution using the Philips Big Bore CT scanner were used in the study. The patients' sCT images were generated using Philips Ingenia MRI scanner with same immobilization accessories used for the CT scans. Patients were scanned with the mDixon method using phased array coils supported by in-built coil bridges in anterior position. Inbuilt MRCAT algorithm was used to convert mDixon MR images to CT equivalent synthetic CT images. MRCAT stands for Magnetic Resonance for Calculating Attenuation [9, 15], algorithm developed by Philips medical systems to create a CT-like density maps from MR images. It has two steps. First, it segmented the images into five discrete segments namely air, fat, water, spongy bone and compact bones. Second, each segment was assigned Hounsfield unit (HU) values (–968 HU), (–86 HU), (42 HU), (198 HU) and (949 HU) for air, fat, water, spongy bone and compact bone, respectively [8]. A detailed description of the MRCAT sCT algorithm is given in a white paper released by Köhler et al. [21].

The difference in the body outline of CT and sCT images were compensated with a water CT number in synthetic CT images to avoid any depth differences and regions of the sCT images which were outside the CT body contour were truncated. The study was performed in an IMPT treatment planning module of the Pinnacle [3] treatment planning system (TPS) Version 16.2 of Philips Medical Systems, Madison, WI, USA. The regular CT data sets were imported into Pinnacle [3] TPS and registered with secondary MRI images. Target and OAR volumes were delineated in the CT image with the MRI T1 and T2 images as secondary image sets. Bilateral beams with 270° and 90° gantry angles with Proteus IBA proton spot scanning machine were used in all plans and pencil beam spots were created with a margin of 1cm around the target volume with spot spacing of 80% profile overlap laterally. The spacing between energy layers were set to 80% of the longitudinal width of the bragg

peak of the subsequent distal layer. A $3 \times 3 \times 3$ mm$^3$ resolution dose grid was defined in the image sets covering the body.

Six plans were created to deliver 72Gy uniform dose to 95% volume of PTVpros+vs with different optimization techniques and parameters as given below:
- nominal multi field optimization without any additional constraints for robustness or beam dose uniformity (Pmfo);
- single field uniform dose optimization with variation constraint set to 3% and 30% weight (P_sfud);
- robust optimization with 5% range error and 3mm setup error in the lateral (X) direction, anterior-posterior (Y) direction, and inferior-superior (Z) direction (P_ro) with 25% weight to all error scenarios;
- robust optimization with 3mm setup error in the lateral(X) direction, anterior-posterior(Y) direction, and inferior-superior(Z) direction with 50% of weight (P_setup);
- robust optimization with 2% range error with 25% weight (P_range2);
- robust optimization with 5% range error with 25% weight (P_range5).

All beams were locked after optimizations to prevent any inadvertent changes to the plans and the plans were copied to sCT image sets using the dynamic planning tool of Pinnacle [3] TPS. All the plan parameters were checked for any deviation from the source plans and ensured to have no differences. The default CT to density table recommended by the MRCAT algorithm vendor [21] and proportional CT to stopping power table were used for dose computation. The plots of tables are given in Figure 1.

CT to stopping power table was derived by applying the proportionality of regular CT scanners' CT to density table to published MRCAT CT to density table to the CT scanners' CT to stopping power table to construct the sCT data sets' stopping power table. The dose grid dimension and resolution of CT image plans were re-created in the in synthetic CT images. Dose was re-computed in the synthetic CT without any changes in the plan.

CT and sCT plans were compared and analyzed for each optimization type for any dose differences using dose volume histogram (DVH), 2D isodose line distribution, homogeneity index, conforma-
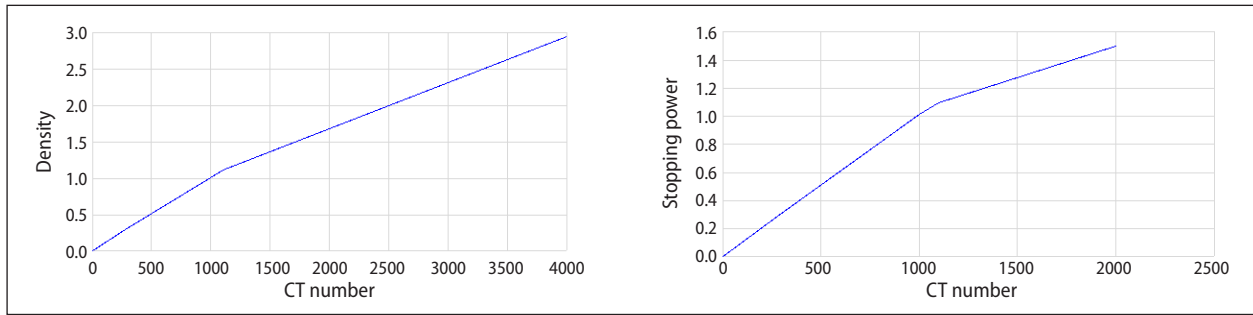
**Figure 1.** CT to density table and CT to stopping power table used for synthetic CT dose computation

tion number and D95 dose to PTVpros+vs volume, bladder and rectum mean doses. 3D gamma analysis was also used to evaluate the dose differences between the plans. Homogeneity index and conformation number were calculated in the PlanIQ system of sun nuclear systems using the formula:

- homogeneity Index (HI):
  *[Dose covering 1% of the specified structure – Dose covering 99% of the specified structure] (Gy)/[Prescription specified dose (Gy)]* [22].
- conformation number (CN) [22]:
  *[72 (Gy), PTVpros+vs]*
  *[The specified structure's volume (cc) covered by specified dose (Gy)²]/[Total volume (cc) covered by specified dose (Gy) × Total volume (cc) of the specified structure]* [22].

Arithmetic mean of differences and standard deviation (SD) of HI and CN were computed. Additionally, the homogeneity Index and conformation number of CT and synthetic CT were analyzed using a two tailed t-test with 5% significance for each optimization technique. A null hypothesis was established as there is no difference in the homogeneity index and conformation number between CT and sCT plans.

Three dimensional doses from regular CT and synthetic plans were exported to Slicer, an open source visualization and analysis tool and gamma analysis were performed. 3% dose difference and 3 mm distance to agreement (DTA) criteria were used for gamma analysis and dose less than 10% of maximum dose was excluded from the analysis.

## Results

Analysis of ten patients shows that P_range2 has similar isodose lines distribution for CT and sCT image sets followed by P_setup and P_range5 plans.

P_range2 plan has identical isodose distribution throughout the beam path and inside the target volume as shown in the Figure 2.

Comparatively, there was a higher level of dose difference observed in Pmfo plans between CT and sCT image sets as shown in Figure 3. Above observations were cross verified with other quantitative parameters to negate any observer biases and explained in the later part of this section.

Dose volume histogram analysis demonstrates the least differences in ROI dose statistics between CT and sCT image sets for P_range2 and P_setup has the highest level of dose differences. Average D95 dose for the PTVpros+vs volume over ten patients for a regular CT plan was 71.51 Gy with 0.78 SD and the recomputed plan on sCT image sets was 71.1 Gy and 0.39 SD for P_range2 plans. On the other hand, P_setup plan has average D95 dose to PTVpros+vs of 70.67 with 1.28 SD and 68.55 with 2.48 SD for CT and sCT image sets, respectively. Differences in average rectal mean dose between image sets was minimal for all the optimization techniques with the highest difference of 0.36 Gy observed for P_ro plans.

Figure 4 displays the DVH plot for all the optimization techniques for an arbitrarily selected patient for CT and sCT plans.

Average difference in mean dose for the bladder between image sets was found to be close to 2 Gy for all the optimization techniques with an exception for P_sfud plans with an average difference of approximately 7 Gy.

Table 1 portrays mean differences of various parameters between CT and sCT datasets optimized with different optimization techniques for ten patient image sets, i.e. the difference in each patient was calculated and its arithmetic average over ten patients was computed. The table also displays the
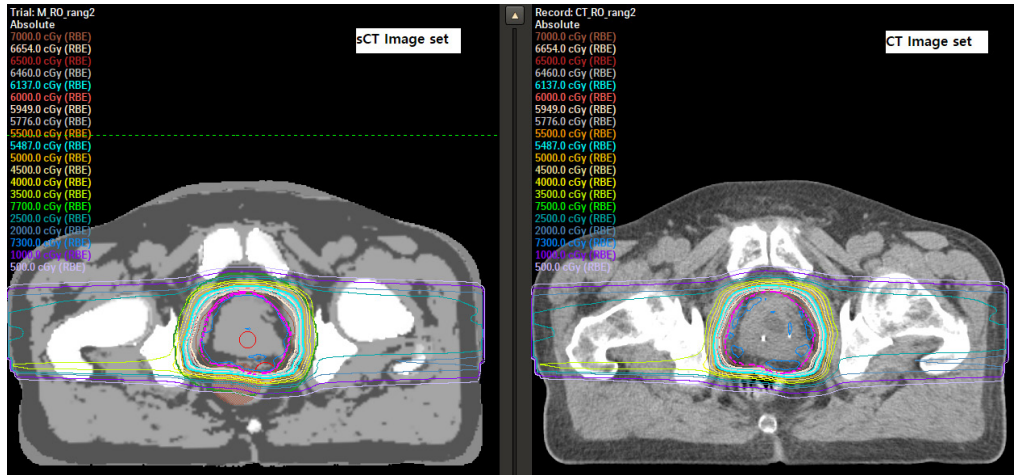
**Figure 2.** 2D Isodose lines display of robustly optimized plan with 2% range error on CT plan and re-computed plan on sCT data set for a randomly chosen patient
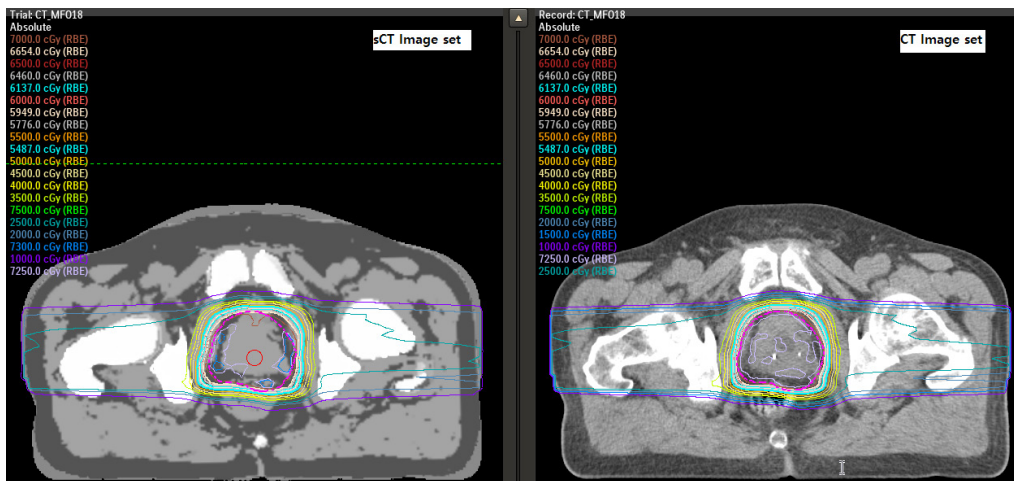


**Figure 3.** 2D Isodose lines display of MFO plan on CT plan and re-computed plan on sCT data set for a randomly chosen patient
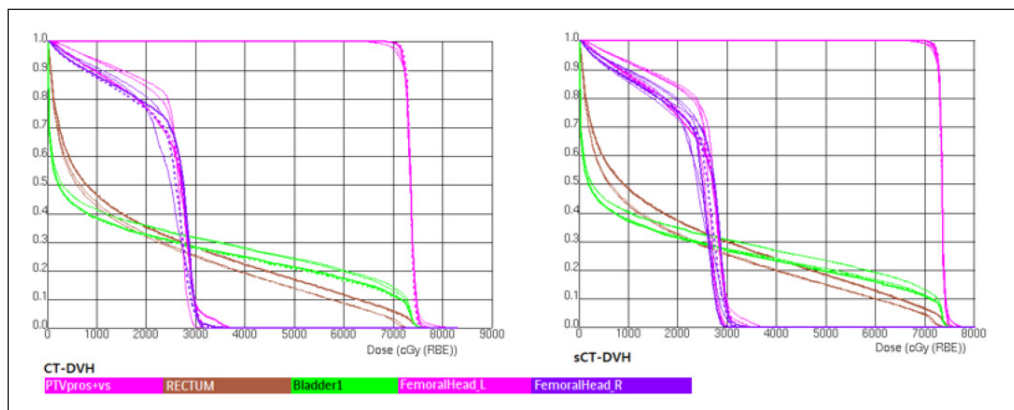


**Figure 4.** The dose volume histogram (DVH) plot of plans optimized with different techniques on the CT image set and dose re-computed on synthetic CT for a randomly chosen patient

**Table 1.** The mean of difference (M Diff) between initial CT and re-computed sCT plans for listed parameters and corresponding standard deviations (SD)

| | P_mfo | | P_ro | | P_range2 | | P_range5 | | P_setup | | P_sfud | |
|---|---|---|---|---|---|---|---|---|---|---|---|---|
| | M Diff | SD | M Diff | SD | M Diff | SD | M Diff | SD | M Diff | SD | M Diff | SD |
| HI [72 (Gy), PTVpros+vs] | 0.045 | 0.030 | 0.023 | 0.023 | 0.017 | 0.014 | 0.024 | 0.014 | 0.045 | 0.032 | 0.022 | 0.045 |
| CN [72 (Gy), PTVpros+vs] | 0.542 | 0.184 | 0.089 | 0.050 | 0.090 | 0.030 | 0.088 | 0.052 | 0.340 | 0.238 | 0.238 | 0.542 |
| Mean dose [Gy] Bladder | 2.099 | 3.797 | 2.283 | 4.069 | 2.032 | 4.044 | 2.077 | 4.031 | 2.031 | 4.053 | 7.008 | 2.099 |
| Mean dose [Gy] Rectum | 0.865 | 0.405 | 0.704 | 0.499 | 0.719 | 0.433 | 0.718 | 0.545 | 0.515 | 0.619 | 1.008 | 0.865 |
| D95 [Gy], PTVpros+vs | 2.139 | 1.463 | 0.676 | 0.31 | 0.873 | 0.577 | 0.750 | 0.461 | 2.123 | 2.008 | 1.005 | 0.490 |

HI — homogeneity index; CN — conformation number

**Table 2.** Results of t-test conducted on every optimization technique on the homogeneity index and conformation number for the ten patients

| | t-test p-values | | | | | |
|---|---|---|---|---|---|---|
| | P_mfo | P_ro | P_range2 | P_range5 | P_setup | P_sfud |
| HI | 0.3558 | 0.6000 | 0.7156 | 0.6345 | 0.3360 | 0.6583 |
| CN | 0.0001 | 0.1004 | 0.1274 | 0.0984 | 0.0245 | 0.0182 |

HI — homogeneity index; CN — conformation number

standard deviation for each parameter. Couple of datasets have shown high differences for most of the parameters impacting the SD significantly.

The homogeneity index and conformation number of ten patients' plans were subjected to t-test for CT plans and sCT plans and results are shown in Table 2. Calculated p values were displayed for each optimization type for the homogeneity index and conformation number.

Table 3 shows the passing percentage of 3D gamma analysis with 3% dose error and 3mm DTA criteria of re-computed sCT plans against the reference CT plans for the ten patients. Mean, standard error and standard deviation of percentage of passing points of ten patients for each optimization technique is computed along with median percentages.

## Discussion

On comparison of different optimization techniques on CT and sCT data sets using isodose lines distribution, DVH, homogeneity index (HI) and conformation number, P_mfo plans show the highest difference in dose profiles. Average HI and CN for P_mfo CT plans were 0.081 and 0.876 against re-computed plans' 0.125 and 0.334, respectively. Mean dose of the bladder had an average difference of 2.1Gy. Gamma analysis shows that P_mfo has the least percentage of points passing for 3% dose error and 3mm DTA criteria with a mean of 94.78% =/−0.57 and median of 95.02%. This could be due to the inherent property of MFO plans to have high gradients and range error difference of sCT were magnified due to the differences in the HU distribution [17, 18].

T-test with p values, 0.0245 and 0.0182 for the confirmation number for P_setup and P_sfud plans, respectively, for PTVpros+vs target volume suggests there is a significant dose difference between CT and sCT data sets inside the structure. Gamma analysis shows P_setup and P_sfud plans has comparatively lesser dose similarity with averages of 94.89% and 94.90% points passing respectively compared to robust optimization plans. There are no statistically significant differences in the HI for the PTVpros+vs volume for these plans. Mean differences in the D95 (Gy), PTVpros+vs were as

**Table 3.** 3D dose gamma analysis results of CT and sCT plans for different optimization techniques for each patient and its mean, standard deviation (SD) standard error (SE), and median percentage values

| Patients | Percentage of points passing for 3% dose error and 3 mm DTA in 3D analysis | | | | | |
|---|---|---|---|---|---|---|
| | P_mfo | P_ro | P_range2 | P_range5 | P_setup | P_sfud |
| P1 | 92.1 | 95.85 | 98.44 | 98.02 | 90.79 | 93.02 |
| P2 | 94.67 | 97.6 | 98.61 | 98.15 | 95.52 | 95.52 |
| P3 | 97.53 | 97.55 | 98.12 | 98.2 | 98.2 | 98.13 |
| P4 | 95.26 | 96.81 | 97.83 | 97.65 | 93.22 | 92.58 |
| P5 | 93.26 | 97.26 | 98.76 | 98.45 | 93.77 | 94.61 |
| P6 | 94.78 | 96.32 | 98.92 | 97.84 | 94.92 | 95.2 |
| P7 | 95.83 | 97.15 | 98.55 | 98.68 | 95.62 | 95.44 |
| P8 | 96.04 | 98.03 | 98.45 | 98.36 | 95.57 | 95.88 |
| P9 | 96.14 | 96.26 | 97.9 | 97.82 | 94.65 | 95.21 |
| P10 | 92.15 | 95.65 | 98.81 | 98.02 | 96.67 | 93.45 |
| Mean | 94.78 | 96.85 | 98.44 | 98.12 | 94.89 | 94.90 |
| SD | 1.79 | 0.80 | 0.38 | 0.32 | 2.01 | 1.61 |
| SE | 0.57 | 0.25 | 0.12 | 0.10 | 0.64 | 0.51 |
| Median | 95.02 | 96.98 | 98.50 | 98.09 | 95.22 | 95.21 |

DTA — distance to agreement

high as 2.12Gy and 1Gy for P_setup and P_sfud plans, respectively. P_sfud plans have mean bladder dose average differences of around 7Gy between CT and sCT image sets.

Manual analysis of isodose lines reveals similar dose pattern inside and outside target volume for RO with 2%, 5% range error plans and RO with 5% range and 3mm setup error between CT and sCT image sets. This was reflected in computed HI and CN numbers as well. Also, these optimization techniques have higher 3D gamma analysis compared to other optimization techniques. P_range2, P_range5 and P_ro plans has average of 98.44%, 98.12% and 96.86% of points passing the 3D gamma with 3% dose error an 3mm DTA criteria. T-test performed for HI and CN with 5% significance level on these optimization technique plans proves there is no significant target dose difference between CT and sCT plans.

Overall analysis of P_range2, P_range5 and P_ro plans portrays range error which was common to all the three optimization types as the key for making the plan less sensitive to spatial HU number differences between CT and sCT plans image sets. Among the optimization techniques with range errors, RO with 2% range error seems the optimization technique with the least dose difference based on the results of all quantitative parameters,

including the homogeneity index, 3D gamma passing percentage, t-test p values and D95 covering PTVpros+vs. Although P_range5 and P_ro plans show good results, higher range error incorporated robust optimization give the impression of an overkill.

Additionally, it was observed that median percentage of points passing for all optimization techniques were above 95% for 3mmDTA and 3% dose difference criteria. Mean percentage of passes were above 95% for all robust optimization techniques and others, too, had pass percentage close to 95% with 94.78% as the least value.

There was a similar study by Maspero et al. which used a multi field optimization technique with the same beam geometries as this study [9]. The study recommended the MR only simulation and treatment planning for IMPT should be clinically implemented only after further studies with a larger patient group [9]. There was another study by Depauw et al. published in 2019 which had the primary objective to assess the clincal suitability of MRCAT sCT images for IMPT treatment planning and strongly recommended sCT images for IMPT treatment planning [15]. The study also used bilateral opposing beams without any range shifter as this study. Daepauw et al. also performed a QA for each field and found all the results above 95%

points passing 3% dose difference and 3mm DTA criteria leaving little room for uncertainty in the beam delivery [15].

## Conclusion

The study clearly demonstrates the possibility of proton optimization techniques to impact the dose differences between CT and synthetic CT image sets and 2% range incorporated robust optimization results in the least dose difference between them, closely followed by 5% range error incorporated robust optimization. Additionally, this study also supports the claims of Nicolas Depauw et al. [15] on the suitability of MRCAT, a synthetic CT image sets based on a mDixon MRI sequence for clinical uses.

At present, there is no published material available to establish the impact of IMPT optimization techniques on sCT prostate image sets' dose accuracy testing. Our study and analysis demonstrate that range error incorporated robust optimization is the suitable optimization technique, which would make the dose computation less susceptible to CT density differences of sCT against the CT image sets.

### Conflict of interest

None declared.

### Funding

None declared.

## References

1. Brock KK, Mutic S, McNutt TR, et al. Use of image registration and fusion algorithms and techniques in radiotherapy: Report of the AAPM Radiation Therapy Committee Task Group No. 132. Med Phys. 2017; 44(7): e43–e76, doi: 10.1002/mp.12256, indexed in Pubmed: 28376237.
2. Beavis AW, Gibbs P, Dealey RA, et al. Radiotherapy treatment planning of brain tumours using MRI alone. Br J Radiol. 1998; 71(845): 544–548, doi: 10.1259/bjr.71.845.9691900, indexed in Pubmed: 9691900.
3. Dowling JA, Sun J, Pichler P, et al. Automatic Substitute Computed Tomography Generation and Contouring for Magnetic Resonance Imaging (MRI)-Alone External Beam Radiation Therapy From Standard MRI Sequences. Int J Radiat Oncol Biol Phys. 2015; 93(5): 1144–1153, doi: 10.1016/j.ijrobp.2015.08.045, indexed in Pubmed: 26581150.
4. Chin AL, Lin A, Anamalayil S, et al. Feasibility and limitations of bulk density assignment in MRI for head and neck IMRT treatment planning. J Appl Clin Med Phys. 2014; 15(5): 4851, doi: 10.1120/jacmp.v15i5.4851, indexed in Pubmed: 25207571.
5. Lee YK, Bollet M, Charles-Edwards G, et al. Radiotherapy treatment planning of prostate cancer using magnetic resonance imaging alone. Radiother Oncol. 2003; 66(2): 203–216, doi: 10.1016/s0167-8140(02)00440-1, indexed in Pubmed: 12648793.
6. Hofmann M, Bezrukov I, Mantlik F, et al. MRI-based attenuation correction for whole-body PET/MRI: quantitative evaluation of segmentation- and atlas-based methods. J Nucl Med. 2011; 52(9): 1392–1399, doi: 10.2967/jnumed.110.078949, indexed in Pubmed: 21828115.
7. Gudur MS, Hara W, Le QT, et al. A unifying probabilistic Bayesian approach to derive electron density from MRI for radiation therapy treatment planning. Phys Med Biol. 2014; 59(21): 6595–6606, doi: 10.1088/0031-9155/59/21/6595, indexed in Pubmed: 25321341.
8. Kirk ML, Tang S, Zhai H, et al. Comparison of prostate proton treatment planning technique, interfraction robustness, and analysis of single-field treatment feasibility. Pract Radiat Oncol. 2015; 5(2): 99–105, doi: 10.1016/j.prro.2014.05.008, indexed in Pubmed: 25413411.
9. Maspero M, van den Berg CAT, Landry G, et al. Feasibility of MR-only proton dose calculations for prostate cancer radiotherapy using a commercial pseudo-CT generation method. Phys Med Biol. 2017; 62(24): 9159–9176, doi: 10.1088/1361-6560/aa9677, indexed in Pubmed: 29076458.
10. Liu Y, Lei Y, Wang Y, et al. MRI-based treatment planning for proton radiotherapy: dosimetric validation of a deep learning-based liver synthetic CT generation method. Phys Med Biol. 2019; 64(14): 145015, doi: 10.1088/1361-6560/ab25bc, indexed in Pubmed: 31146267.
11. Uh J, Merchant TE, Li Y, et al. MRI-based treatment planning with pseudo CT generated through atlas registration. Med Phys. 2014; 41(5): 051711, doi: 10.1118/1.4873315, indexed in Pubmed: 24784377.
12. Chen L, Price R, Wang L, et al. MRI-based treatment planning for radiotherapy: Dosimetric verification for prostate IMRT. Int J Radiat Oncol Biol Phys. 2004; 60(2): 636–647, doi: 10.1016/s0360-3016(04)00960-5, indexed in Pubmed: 15380601.
13. Eilertsen K, Vestad LN, Geier O, et al. A simulation of MRI based dose calculations on the basis of radiotherapy planning CT images. Acta Oncol. 2008; 47(7): 1294–1302, doi: 10.1080/02841860802256426, indexed in Pubmed: 18663645.
14. Prabhakar R, Julka PK, Ganesh T, et al. Feasibility of using MRI alone for 3D radiation treatment planning in brain tumors. Jpn J Clin Oncol. 2007; 37(6): 405–411, doi: 10.1093/jjco/hym050, indexed in Pubmed: 17635965.
15. Depauw N, Keyriläinen J, Suilamo S, et al. MRI-based IMPT planning for prostate cancer. Radiother Oncol. 2020; 144: 79–85, doi: 10.1016/j.radonc.2019.10.010, indexed in Pubmed: 31734604.
16. Unkelbach J, Bortfeld T, Martin BC, et al. Reducing the sensitivity of IMPT treatment plans to setup errors and range uncertainties via probabilistic treatment planning. Med Phys. 2009; 36(1): 149–163, doi: 10.1118/1.3021139, indexed in Pubmed: 19235384.
17. Quan EM, Liu W, Wu R, et al. Preliminary evaluation of multifield and single-field optimization for the treat-

ment planning of spot-scanning proton therapy of head and neck cancer. Med Phys. 2013; 40(8): 081709, doi: 10.1118/1.4813900, indexed in Pubmed: 23927306.

18. Unkelbach J, Paganetti H. Robust Proton Treatment Planning: Physical and Biological Optimization. Semin Radiat Oncol. 2018; 28(2): 88–96, doi: 10.1016/j.semradonc.2017.11.005., indexed in Pubmed: 29735195.

19. Liu W, Frank SJ, Li X, et al. PTV-based IMPT optimization incorporating planning risk volumes vs robust optimization. Med Phys. 2013; 40(2): 021709, doi: 10.1118/1.4774363, indexed in Pubmed: 23387732.

20. Pugh TJ, Amos RA, John Baptiste S, et al. Multifield optimization intensity-modulated proton therapy (MFO-IMPT) for prostate cancer: Robustness analysis through simulation of rotational and translational alignment errors. Med Dosim. 2013; 38(3): 344–350, doi: 10.1016/j.meddos.2013.03.007, indexed in Pubmed: 23747223.

21. Köhler M., Vaara T., Van Grootel M. et al. MR-only simulation for radiotherapy planning, White paper: Philips MRCAT for prostate dose calculations using only MRI data; 2015. http://incenter.medical.philips.com/doclib/enc/fetch/2000/4504/577242/577251/587787/White_Paper_MR-only_sim_LR.pdf%3Fnodeid%3D11147198%26vernum%3D-2.

22. Gintz D, Latifi K, Caudell J, et al. Initial evaluation of automated treatment planning software. J Appl Clin Med Phys. 2016; 17(3): 331–346, doi: 10.1120/jacmp.v17i3.6167, indexed in Pubmed: 27167292.